Biochemistry and Biophysics Reports 37 (2024) 101653

Contents lists available at ScienceDirect

Biochemistry and Biophysics Reports

journal homepage: www.elsevier.com/locate/bbrep

Cellular-level analyses of *SCN5A* mutations in left ventricular noncompaction cardiomyopathy suggest electrophysiological mechanisms for ventricular tachycardia

Yanfen Li [a], Shenghua Liu [a], Jian Huang [a], Yuanyuan Xie [a], Aijie Hou [b,**], Yingjie Wei [a,*]

[a] State Key Laboratory of Cardiovascular Disease, Fuwai Hospital, National Center for Cardiovascular Diseases, Chinese Academy of Medical Sciences and Peking Union Medical College, Beijing, 100037, People's Republic of China

[b] Department of Cardiology, The People's Hospital of China Medical University, The People's Hospital of Liaoning Province, No. 33, Wenyi Road, Shenhe District, Shenyang City, Liaoning Province, 110016, People's Republic of China

ARTICLE INFO

Keywords:
SCN5A
Variant
LVNC
Arrhythmia
Tachycardia

ABSTRACT

Left ventricular noncompaction cardiomyopathy (LVNC) is a cardiovascular disease characterized by arrhythmia and heart failure. In this study, LVNC myocardial samples were collected from patients who underwent heart transplantation and were analyzed using exome sequencing. Approximately half of the LVNC patients carried *SCN5A* variants, which are associated with clinical symptoms of ventricular tachycardia. To investigate the electrophysiological functions of these *SCN5A* variants and the underlying mechanism by which they increase arrhythmia susceptibility in LVNC patients, functional evaluations were conducted in CHO–K1 cells and human embryonic stem cell-derived cardiomyocytes (hESC-CMs) using patch-clamp or microelectrode array (MEA) techniques. These findings demonstrated that these *SCN5A* mutants exhibited gain-of-function properties, leading to increased channel activation and enhanced fast inactivation in CHO–K1 cells. Additionally, these mutants enhanced the excitability and contractility of the cardiomyocyte population in hESC-CMs models. All *SCN5A* variants induced fibrillation-like arrhythmia and increased the heart rate in cardiomyocytes. However, the administration of Lidocaine, an antiarrhythmic drug that acts on sodium ion channels, was able to rescue or alleviate fibrillation-like arrhythmias and secondary beat phenomenon. Based on these findings, it is speculated that *SCN5A* variants may contribute to susceptibility to arrhythmia in LVNC patients. Furthermore, the construction of cardiomyocyte models with *SCN5A* variants and their application in drug screening may facilitate the development of precise therapies for arrhythmia in the future.

1. Introduction

Left ventricular non-compaction (LVNC) is a rare congenital cardiomyopathy characterized by excessive trabeculations in the apical and lateral walls of the left ventricle during early embryonic heart development [1]. The main examination methods were echocardiography and magnetic resonance imaging. The lesions involved both the left ventricle and the right ventricle, leading to ventricular systolic and diastolic dysfunction, progressive heart failure, malignant arrhythmia, and thromboembolism in the clinic [2–7]. Ventricular arrhythmias ranging from premature ventricular beats to ventricular tachycardia and fibrillation have been reported in isolated LVNC patients [8]. However, the mechanism of malignant ventricular arrhythmia in LVNC patients remains unclear, and there is no special treatment method for LVNC.

The *SCN5A* gene encodes a major cardiac voltage-gated sodium channel called NaV1.5, which mediates the sodium ion permeability of cardiac cells and maintains the normal function of the inward sodium current (I_{Na}). The I_{Na} current predominates action potential initiation and propagation, which involves and is involved in the excitation–contraction coupling cascade and proper conduction of electrical impulse within the heart [9]. The alpha subunit contains four homologous domains (I, II, III, IV), as well as an intracellular N-terminus and a C-terminus segment. The four domains form a pore to conduct Na^+ ions across the cell membrane and attach to one another by cytoplasmic linker sequences with key residues for channel inactivation gating. The four S4 segments make up the voltage sensor and are responsible for

* Corresponding author.
** Corresponding author.
E-mail addresses: 1758624242@qq.com (A. Hou), Weiyingjie@fuwaihospital.org (Y. Wei).

https://doi.org/10.1016/j.bbrep.2024.101653
Received 29 October 2023; Received in revised form 22 January 2024; Accepted 24 January 2024

increasing channel permeability during membrane depolarization [10,11]. The S5 and S6 segments (p-loops) of each domain constitute the pores of the channel and are responsible for the channel's selectivity filter [12]. *SCN5A* heterozygous variants have been associated with arrhythmias, cardiac conduction disorders, and structural cardiomyopathy [13]. This is partly because *SCN5A* variations can disrupt electrical activity in heart muscle cells by altering the electrophysiological properties of the channel, such as activation and fast inactivation. Additionally, the slow inactivation of hNaV1.5 channels can also impact the excitability and conduction speed of heart muscle cells. For instance, Vilin demonstrated that a mutation in *SCN5A* significantly decreases slow inactivation, which increases the likelihood of arrhythmias in patients [14].

The purpose of this paper was to examine the electrophysiological mechanisms of LVNC patients with *SCN5A* mutations who are susceptible to ventricular tachycardia or even ventricular fibrillation and to analyze the impact of *SCN5A* mutations on cardiomyocyte excitability and contractility through the use of whole-cell patch clamp and multi-electrode array (MEA) techniques.

2. Materials and methods

2.1. Exome sequencing and analysis

LVNC myocardial samples were collected from patients who underwent heart transplantation (HTx) at Fuwai Hospital and fulfilled defined diagnostic criteria as determined by pathologists [15]. Control samples were collected from accident donors with no history of heart disease or without heart disease confirmed by surgeons and pathologists. Exomes were evaluated with an AgilentSure Select Human All Exon V6 Kit and sequenced with one lane per sample via Illumina HiSeq X. ANNOVAR software was used to analyze all genetic variants. The variant frequency in the population was annotated in dbSNP147, 1000 Genomics, and ExAC. *SCN5A* variants were further verified by Sanger sequencing.

Disease history and pedigree information were obtained according to the records of the clinicians. The participants provided written informed consent. Fuwai Hospital's Institutional Ethical Review Board approved this study, which conforms to the Helsinki Declaration guidelines.

2.2. Immunohistochemistry and immunofluorescence

Immunohistochemistry was performed on the myocardial tissue using a standardized protocol. The tissue was first fixed with neutral buffered formalin and then embedded in paraffin. Subsequently, dehydration was carried out using alcohol and xylene, followed by sealing with 0.05 % hydrogen peroxide. The immunofluorescence procedure employed in this study was consistent with the methodology described in a previous article [16]. Immunohistochemistry and immunofluorescence images were acquired utilizing a Leica DM750 microscope and a Leica Sp8 confocal scanning laser microscope, respectively.

2.3. Plasmid construction and virus packaging

To assess the functionality of the mutant NaV1.5, EGFP-tagged wild-type *SCN5A* and its variants were inserted into the pAD-CMV-MCS-EGFP-3FLAG adenoviral vector with the restriction enzymes Kpn1 and *Eco*RV. The plasmids were subsequently validated through sequencing. The adenoviral plasmid was subsequently amplified, isolated, and transfected into HEK293 cells using Lipofectamine 3000 (Invitrogen). Four hours after transfection, the cells were cultured in DMEM supplemented with 10 % FBS. After eight days, the cells were collected and centrifuged. Next, the recombinant adenovirus lysates were amplified and purified. The HEK293 cells were infected with the cell lysate, and the collection process was repeated to obtain higher titer viral stocks. The viral titer was determined by calculating the number of plaque-forming units (PFUs) per milliliter.

2.4. Cell culture and transfection

A cell bank (National Biomedical Experimental Cell Resource Bank, Beijing, China) was used to establish the Chinese hamster ovary (CHO) cell line, which was grown in a mixture of 50 % DMEM and 50 % F-12 medium (Gibco, Carlsbad, CA, USA) supplemented with 10 % fetal bovine serum. Lipofectamine reagent (Invitrogen, Carlsbad, CA, USA) was used to transfect the plasmids into CHO–K1 cells. After 6 h, the transfection mixture was discarded, and the mixture was replaced with 1.5 ml of fresh DMEM/F12 medium containing 10 % FBS in each well. The cells were digested after 48 h and plated on dishes coated with poly-L-lysine for electrophysiological testing.

2.5. HESCs culture and cardiomyocyte differentiation

The human embryonic stem cell (hESC) line (Cellapy, Beijing, China) was cultured in PSCeasy hESC/iPSC medium (CA1001500; Cellapy).The cells were passaged every 3–4 days at 70–80 % confluence using 0.5 mM EDTA (Cellapy, Beijing, China) in a 37 °C and 5 % CO_2 incubator. Human embryonic stem cells (hESCs) were differentiated into cardiomyocytes according to a previously published protocol with certain adjustments [17]. For this purpose, a commercially available CardioEasy cardiac differentiation kit (CA2004500; Cellapy) was used. After reaching a confluency of approximately 70–80 %, the human embryonic stem cells (hESCs) were exposed to induction medium I. Subsequently, after a period of 48 h, the cells were transferred to induction medium II for an additional 48 h. Induction Medium III was subsequently utilized, with regular refreshment every other day. Notably, between days 7 and 9, the cells exhibited contraction, indicating successful differentiation into cardiomyocytes. Cardiomyocytes derived from embryonic stem cells (hESC-CMs) were subsequently exposed to a period of glucose deprivation for three days. The non-cardiomyocytes gradually died when cultured in the presence of CardioEasy Human Myocardial Purified Complete Medium from CELLAPY (Beijing, China), leading to the isolation of purified differentiated cardiomyocytes (hESC-CMs). Subsequently, the culture medium was replaced to prepare for subsequent experimentation.

2.6. Electrophysiology

The sodium current was captured by an Axopatch 700B amplifier (Axon Instruments, Burlingame, CA, USA). The glass electrode was drawn using borosilicate glass capillaries. The glass electrode resistance was 1.5–2.5 M. The intracellular solution of CHO–K1 was accurately prepared (140 CsF, 10 HEPES, 10 NaCl, 1.1 EGTA, and 20 glucose in mmol/L), the pH was adjusted to 7.3 with cesium hydroxide, and the mixture was sterilized and filtered. For the recording bath solutions for CHO–K1 cells, the following components were included at millimolar concentrations: 10 HEPES, 140 NaCl, 1 $MgCl_2$, 1 $CaCl_2$, 3 KCl, and 20 glucose. The pH of the solution was adjusted to 7.3 using sodium hydroxide. The following glass electrode was used as the intracellular solution for hESC-CMs (in mmol/L): 150 KCl, 10 HEPES, 5 NaCl, 2 $CaCl_2$, 5 EGTA, and 5 MgATP (pH 7.2 adjusted by potassium hydroxide); the following bath or extracellular solutions were used (in mmol/L): 148 NaCl, 15 HEPES, 1 $MgCl_2$, 5.4 KCl, 0.4 NaH_2PO_4, 1.8 $CaCl_2$, and 5.5 glucose (pH 7.4 adjusted by sodium hydroxide).

2.7. Extracellular field potential and impedance records of cardiomyocytes

This study focused on investigating the functions of human embryonic stem cell-derived cardiomyocytes (hESC-CMs) in a two-dimensional monolayer culture. The hESC-CMs were cultured at a density of 50,000 cells per well and placed on a Cardio Excel plate reader (Nanion CE-96) according to the manufacturer's instructions. Prior to adenovirus transfection, the hESC-CMs formed a syncytial monolayer.

The electrophysiological and phenotypic characteristics of the cells were assessed by continuously recording impedance and the external field potential. After 5 days, the cells were infected with pAD-*SCN5A* variants, including wild-type (WT) and EGFP control adenoviruses. Three separate wells were tested for each group, and the culture medium was changed every 24 h. After 24 h, the test wells were supplemented with Lidocaine. This was achieved by removing 5 % of the media volume and replacing it with an equivalent volume of a freshly prepared Lidocaine solution, which had a concentration 20 times greater than the desired final concentration in the maintenance media. The prepared solution was stored in an incubator at 37 °C and a CO_2 concentration of 5 % until it was added to the test wells. After a 30-min incubation period, the signals in each well were normalized to the baseline values before comparisons were made. Throughout the entire process, the field potential and the number of beats were continuously detected and recorded.

2.8. Data and statistical analysis

The statistical analysis and data used are in line with the instructions for the pharmacological experimental design and analysis. The patch clamp data were processed with Clampfit 10.4 software and analyzed with Graph Pad Prism 5.0 software. The maximum inward current values obtained from the activation protocols were transformed into conductance values using formula $G = I/(V–V_{Na})$. V_{Na} represents the reversal potential of sodium currents. To assess the inactivation of these channels, the peak current following various prepulses was normalized and graphed as a function of voltage. Both activation and inactivation curves were fitted by the Boltzmann equation: Y=Bottom +(Top–Bottom)/(1+exp [($V_{1/2}$ –V m)/k]), where $V_{1/2}$ represents the voltage at which half of the maximum current or conductance was acquired. In this equation, Y represents G/G_{max} or I/I_{max}, and k represents the slope factor. The monoexponential recovery curves were utilized to fit the data according to equation $I/I_{max} = A_1[1\text{-}exp(-t/\tau_1)]$. The $V_{1/2}$ values of the activation (V_{hact}), fast inactivation ($V_{Fhinact}$), slow inactivation ($V_{Shinact}$) and time constant (τ) for the recovery from inactivation obtained with each construct are presented in Table S1 and Table S2. Statistical comparisons were conducted using one-way analysis of variance (ANOVA). A P value < 0.05 was considered to indicate statistical significance. The legends in the figures provide detailed information.

3. Results

3.1. Frequency of SCN5A variants in LVNC patients

In this study, *SCN5A* variants were identified in 44.4 % of the 27 patients analyzed. The distributions of these variants are summarized in Table 1. The most common abnormal clinical arrhythmia observed was ventricular tachycardia. A total of seven heterozygous single-nucleotide variants (p.G292S–*SCN5A*, p.H558R–*SCN5A*, p.P1090L-*SCN5A*, p.R1195H–*SCN5A*, p.R1193Q-*SCN5A*, p.A1180V–*SCN5A*, and p.V1951L-*SCN5A*) were identified. The location of these *SCN5A* variants on the linear topology of the cardiac sodium channel α subunit is depicted in Fig. 1A. Six of the variants were found in intracellular transmembrane segments, while the p.G292S–*SCN5A* variant was located in the extracellular transmembrane segments between S5 and S6 (P-loops). These P-loops form the channel pore and regulate ion selectivity and permeation. It is hypothesized that these variants may alter the biophysical properties of the channel. The variants were confirmed through Sanger sequencing, as shown in Fig. 1B. Additionally, an electrocardiogram of a patient with left ventricular noncompaction carrying the V1951L mutation is presented, revealing ventricular tachycardia (Fig. 1C).

Table 1
Summary of *SCN5A* variants detected in 27 LVNC patients.

SCN5A variants	Genomic location	Clinical significance	Patient ID	Clinical features
p.G292S-*SCN5A*	chr3:38603948; rs3918389 c.874C > T	uncertain-significance	8	Ventricular tachycardia; Atrial tachycardia; Sinus tachycardia, Atrioventricular block, QT interval prolongation
p.H558R-*SCN5A*	chr3:38603929; rs1805124 c.1673T > C	Benign/Likely benign	5,6,7	Ventricular tachycardia; Atrial tachycardia
p.P1090L-*SCN5A*	chr3:38579455; rs1805125C.3269G > A	Benign/Likely benign	11	Paroxysmal ventricular tachycardia; T wave abnormality
p.A1180V–*SCN5A*	chr3:38575424; rs41310765 c.3539G > A	uncertain-significance	9	Ventricular tachycardia; Incomplete right bundle branch block; T wave abnormality; QT interval prolongation
p.R1195H-*SCN5A*	chr3:38575379 rs199473596 c.3584C > T	Uncertain significance	12	Ventricular tachycardia; Ventricular premature contractions, Abnormal Q waves, ST-T changes, QT interval prolongation
p.R1193Q-*SCN5A*	chr3:38575385; rs41261344 c.3578C > T	Likely benign|Benign	1,2,3,4	Ventricular tachycardia; ST-T changes; QT interval prolongation
p.V1951L-*SCN5A*	chr3:38550521; rs41315493 c.5851C > A	Likely benign|Benign	10	Ventricular tachycardia; ST-T changes

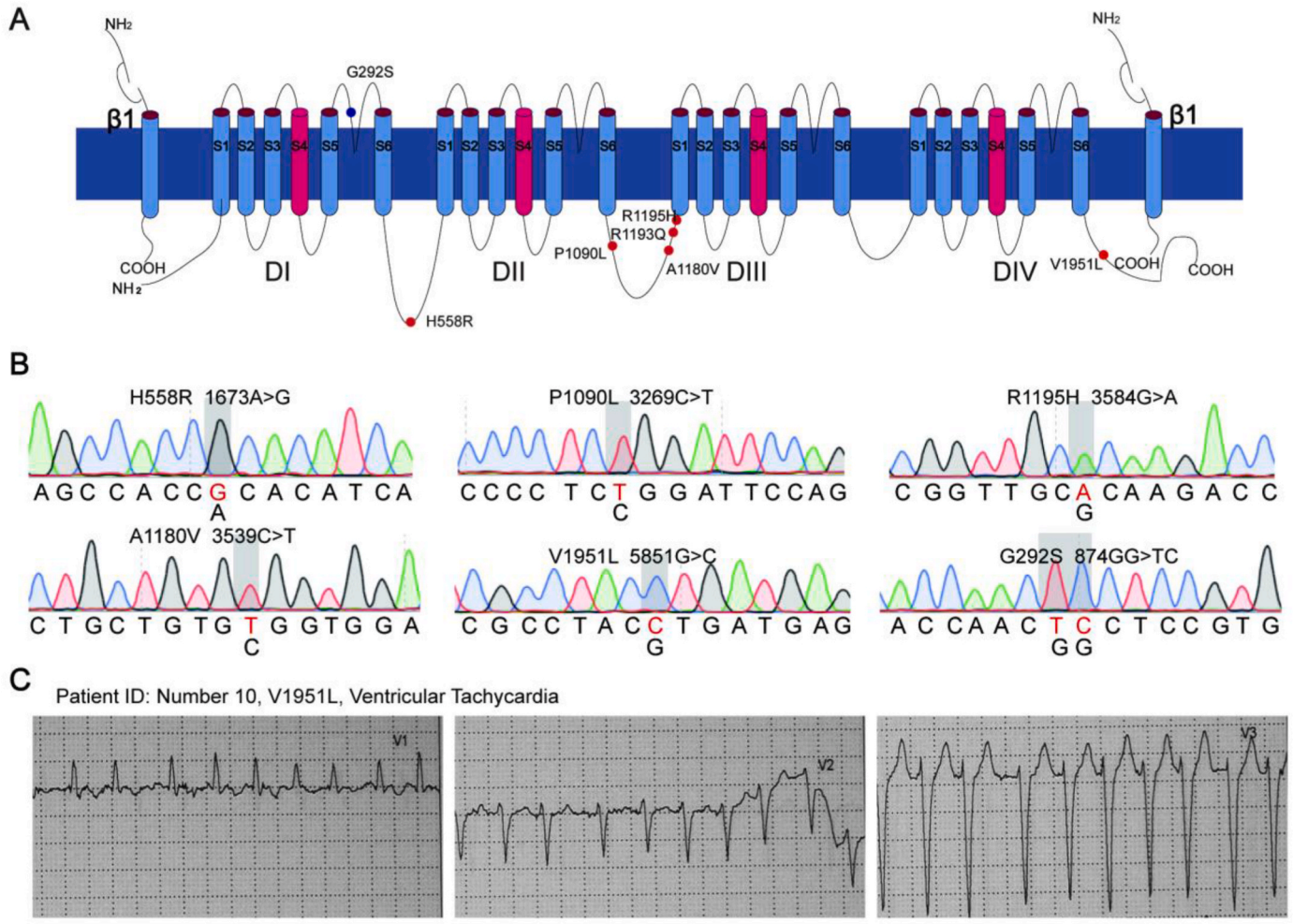

Fig. 1. Topologic location of *SCN5A* variants and sequence analysis of the constructed SCN5A variants
A The α subunit of the *SCN5A* cardiac sodium channel is a transmembrane protein with four domains. The red points (•) represent seven heterozygous variants (p.G292S–*SCN5A*, p.H558R–*SCN5A*, p.P1090L-*SCN5A*, p.R1195H–*SCN5A*, p.R1193Q-*SCN5A*, p.V1951L-*SCN5A*, p.R1193Q-*SCN5A* and p.A1180V–*SCN5A*) located in intracellular loops, and the blue points (•) represent the heterozygous variant p.G292S–*SCN5A* located in extracellular loops. **B** Sequence analysis of the constructed *SCN5A* variants. **C** Electrocardiograms of a LVNC patient carrying the V1951L mutation.

3.2. Localization and distribution of NaV1.5 in cardiac muscle fiberss and hESC-CMs

To determine the distribution of NaV1.5 in the LVNC myocardium, immunohistochemistry was applied to sample sections from the left ventricular myocardium. NaV1.5 was located in the disorganized T-tubules and intercalated discs in the LVNC tissues, consistent with the findings in the normal sample (Fig. 2A). The NaV1.5 protein was shown to be associated mainly with N-cadherin and actin proteins on the membrane of hESC-CMs by immunofluorescence staining. The H558R, P1090L, and V1951L variants caused an increase in hNaV1.5 channel proteins in the nucleus and cytoplasm, and the distributions of N-CAD and actin were also disrupted (Fig. 2B).

3.3. The effects of various variants on the activation of the NaV1.5 channel

To evaluate the effects of the variant on the activation of the NaV1.5-α subunit, we expressed WT and mutant NaV1.5-α in CHO–K1 cells and conducted electrophysiological experiments using the whole-cell patch-clamping technique. We calculated the G-V curves (steady-state activation) of INa. The Vhact values of the p.R1195H–*SCN5A* and p.V1951L-*SCN5A* mutant channels were negatively shifted by 20.22 mV and 12.00 mV, respectively (p.R1195H–*SCN5A*: n = 4, ****P < 0.001; p.V1951L-*SCN5A*: n = 6, ****p < 0.01; & WT: n = 6). Similarly, compared with those of the WT, the Vhact values of the remaining variants (p.G292S–*SCN5A*, p.H558R–*SCN5A*, and p.A1180V–*SCN5A*) were also slightly negatively related (Fig. 3A–C). The mean values of the midpoint (Vhact) of the activation curves for the WT and variant channels are provided in Table S1. Hence, these mutations likely have a gain-of-function effect on NaV1.5 channels by enhancing channel activation.

3.4. The effects of the variants on the fast inactivation of the NaV1.5 channel

The fast inactivation characteristics of the *SCN5A* variants were examined and compared with those of the WT channel. The amplitude of the test pulse was standardized by normalizing it to the maximum recorded current during the prepulse. This normalized amplitude was then plotted against the voltage of the prepulse to generate a voltage-dependent inactivation curve. Subsequently, the curve was fitted to a standard Boltzmann function. The VFhinact values of the p.R1195H–*SCN5A*, p.V1951L-*SCN5A* and p.R1193Q-*SCN5A* channels were negatively shifted by 11.71 mV, 5.23 mV and 6.35 mV, respectively. (p.R1195H–*SCN5A*: n = 6, ****P < 0.0001; p.V1951L-*SCN5A*: n = 6, ****p < 0.0001; p.R1193Q-*SCN5A*: n = 7, ****p < 0.0001, & WT:

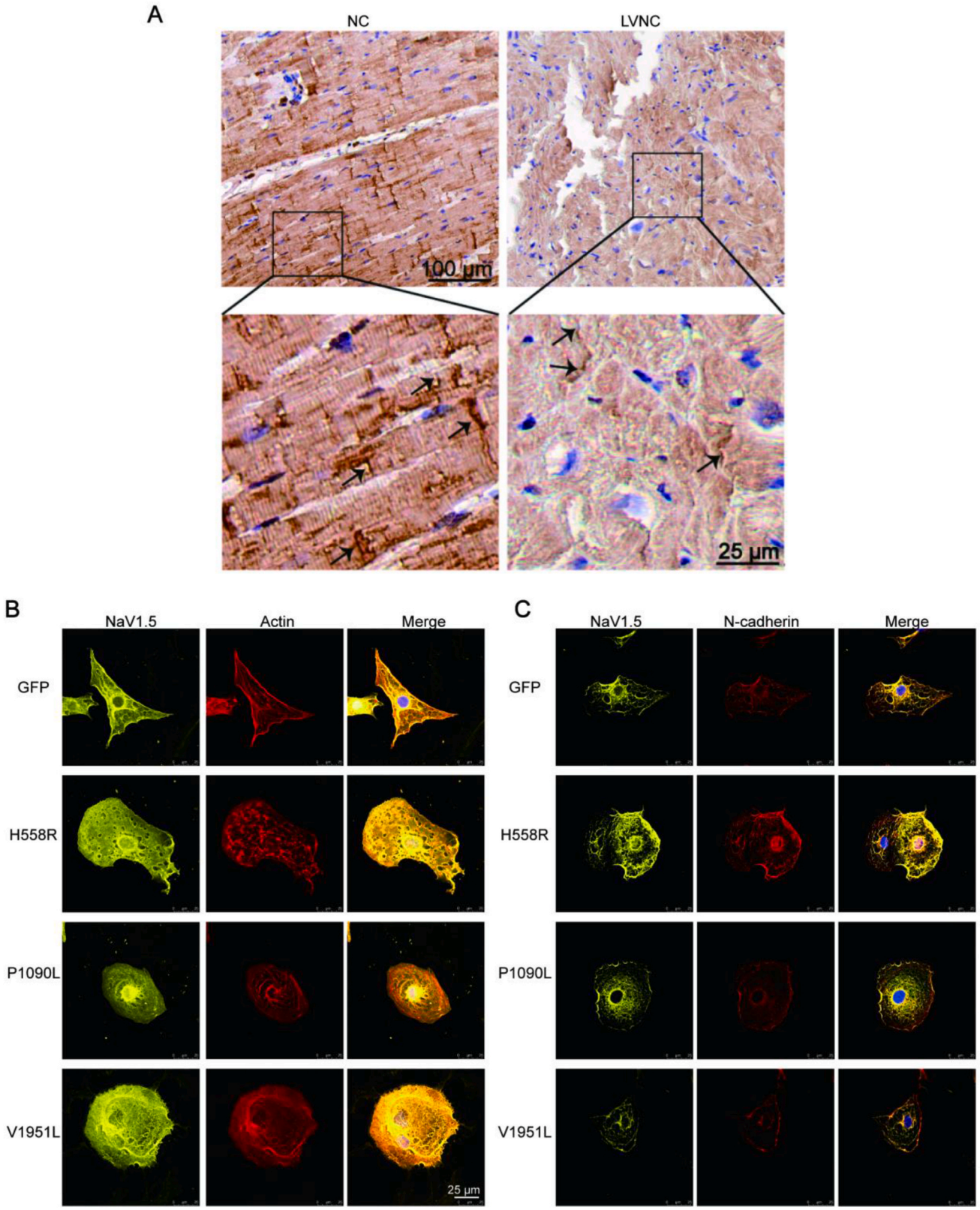

Fig. 2. Location and expression of NaV1.5 in human cardiac tissues and hESC-CMs.
A Immunohistochemistry was used to evaluate the distribution of the NaV1.5 protein in both normal human hearts and left ventricular noncompaction (LVNC) tissues. The localization of NaV1.5 in the T-tubule system and intercalated discs is indicated by black arrows in the representative images. The upper panels contain a box delineating the regions that are magnified in the lower panels. Scale bars measuring 100 μm and 25 μm are provided in the upper and lower panels, respectively. $n > 3$ for each group. **B** Images of immunofluorescence staining for actin (red), NaV1.5 (yellow), N-cadherin (red), and NaV1.5 (yellow) proteins (in the right panels) in hESC-CMs transfected with *SCN5A* variants or an empty virus.

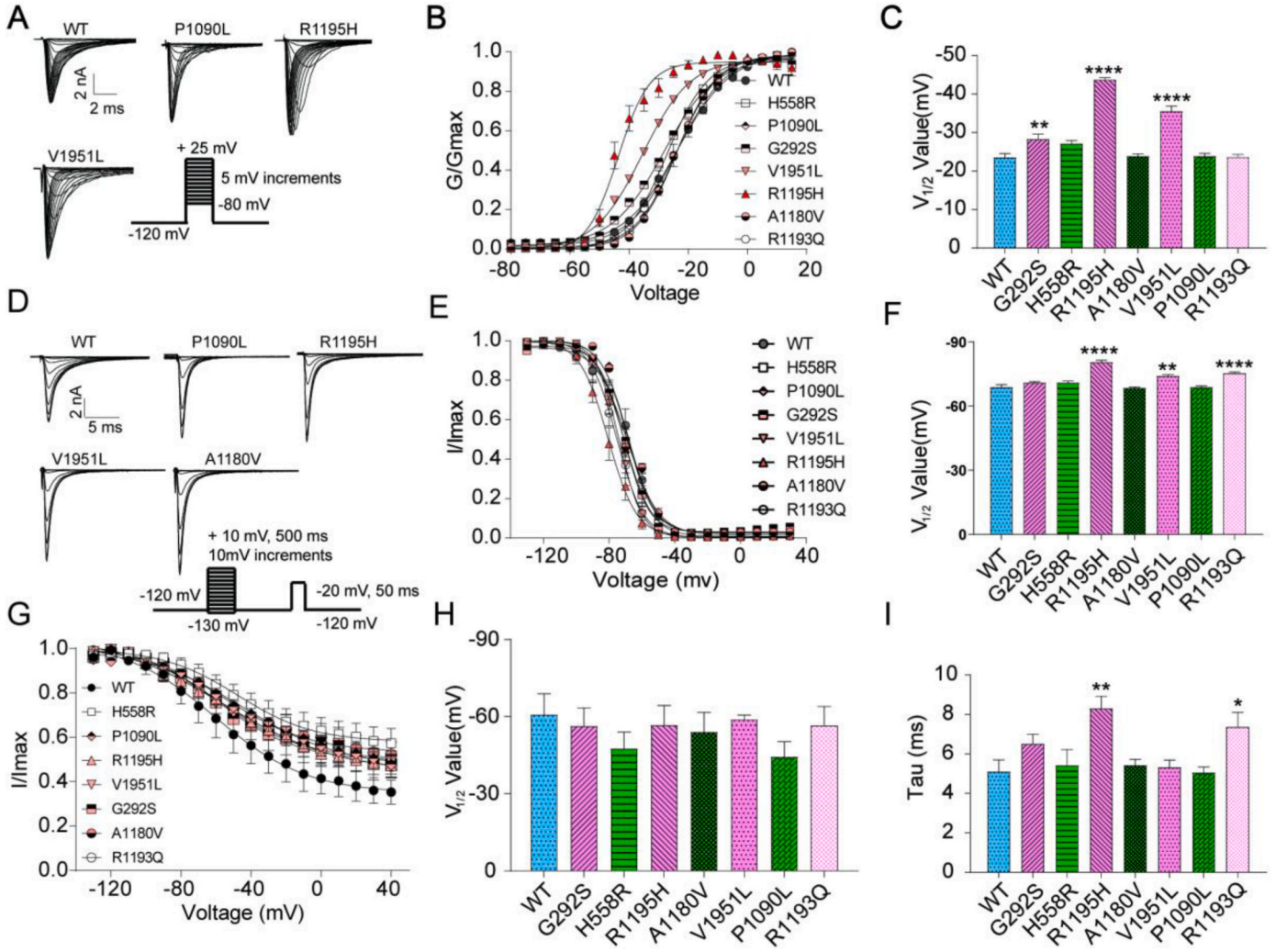

Fig. 3. Analysis of the SCN5A variants in CHO–K1 cells.
A Representative whole-cell current traces of WT and variant sodium channel currents. (Inset) The recording protocol. The experimental protocol consisted of applying different depolarizing potentials ranging from −80 mV to +15 mV, starting from a resting potential of −120 mV. The stimulus frequency used was 0.5 Hz to elicit the recorded currents. **B** Activation curves of the WT or variant channels. **C** Bar graphs showing the $V_{1/2}$ values of the activation curves for the WT and variant strains. **D** Representative steady-state fast inactivation current traces of WT NaV1.5 channels and variants. **E** The steady-state fast inactivation curves exhibit a dependence on voltage. **F** $V_{1/2}$ values summarized from panel E. **G** Voltage-dependent characteristics of the steady-state slow inactivation curves of variant or wild-type channels. **H** Recovery of WT and variant channels from inactivation. **I** Bar graph showing the recovery time constant τ (ms). The details are provided in Table S1.

n = 7). The VFhinact values of the p.G292S–*SCN5A* and H558R channels were also slightly negatively shifted by 2.10 mV and 2.07 mV, respectively. The V1/2 values of the p.P1090L-*SCN5A* channel and the p.A1180V–*SCN5A* channel were not affected (Fig. 3D–F; Table S1).

3.5. *The effects of the variants on the slow inactivation and recovery of the NaV1.5 channel*

Slow inactivation of NaV1.5 channels can affect the excitability and conduction velocity of cardiomyocytes [19–21]. Therefore, by first administering 10-s depolarization pulses and then a 50-ms hyperpolarization pulse to −120 mV, the voltage-dependent nature of the steady-state delayed inactivation was evaluated. This approach made it possible to determine the channel availability by allowing the channels to recover from quick inactivation prior to the test pulse. assuming that 3 s of recovery at −120 mV is enough to prime the NaV1.5. During the slow inactivation research, a set 13-s pulse duration was applied to 5 channels after the 10-s prepulses. Under these test conditions, six variants shifted in the depolarizing direction on the slow inactivation curve (Fig. 3G). These findings imply that these mutations all reduced the slow inactivation of the Na^+ channel. The decrease in the rate of slow inactivation may contribute to the propensity of patients carrying these mutants to experience arrhythmia. Although there was no statistically significant difference (variant channels: n ≥ 5 vs. WT: n = 6, ns, P > 0.05), the mean values of the midpoint (Vshinact) of the slow inactivation curves for the WT and six variant sodium channels are provided in Table S1.

NaV1.5 exhibits a reduction in slow inactivation, corresponding to duration-dependent bi-exponential recovery, which is commonly associated with various arrhythmia syndromes [20]. Hence, we investigated the recovery status of the six variants from the inactivation. Prior to quantifying the number of available channels using a standard test pulse to −20 mV for 50 ms, a 100 ms inactivating prepulse to −20 mV was applied to allow the channel to reach a steady state of inactivation. Subsequently, a recovery period of varying durations (ranging from 0.1 ms to 10 s) at −120 mV was implemented. The results of our study indicate that the p.R1195H–*SCN5A* and p.R1193Q-*SCN5A* variations had notable impacts on the ability of NaV1.5 channels to recover from inactivation. Specifically, the channels harboring the p.R1195H–*SCN5A* and p.R1193Q-*SCN5A* variants demonstrated a slower recovery rate

than did the channels harboring the wild-type variant (Fig. 3H–I). The specific time constants of recovery from inactivation are provided in Table S1.

3.6. Effects of SCN5A variants on the excitability and contractility of the cardiomyocyte population

To evaluate the excitability of cardiomyocytes with variants, we tested and analyzed their excitability and contractility by examining changes in the beat rate and amplitude of cardiomyocytes infected with adenovirus (pAD-CMV-*SCN5A*-EGFP-3FLAG). After infection for 48 h,

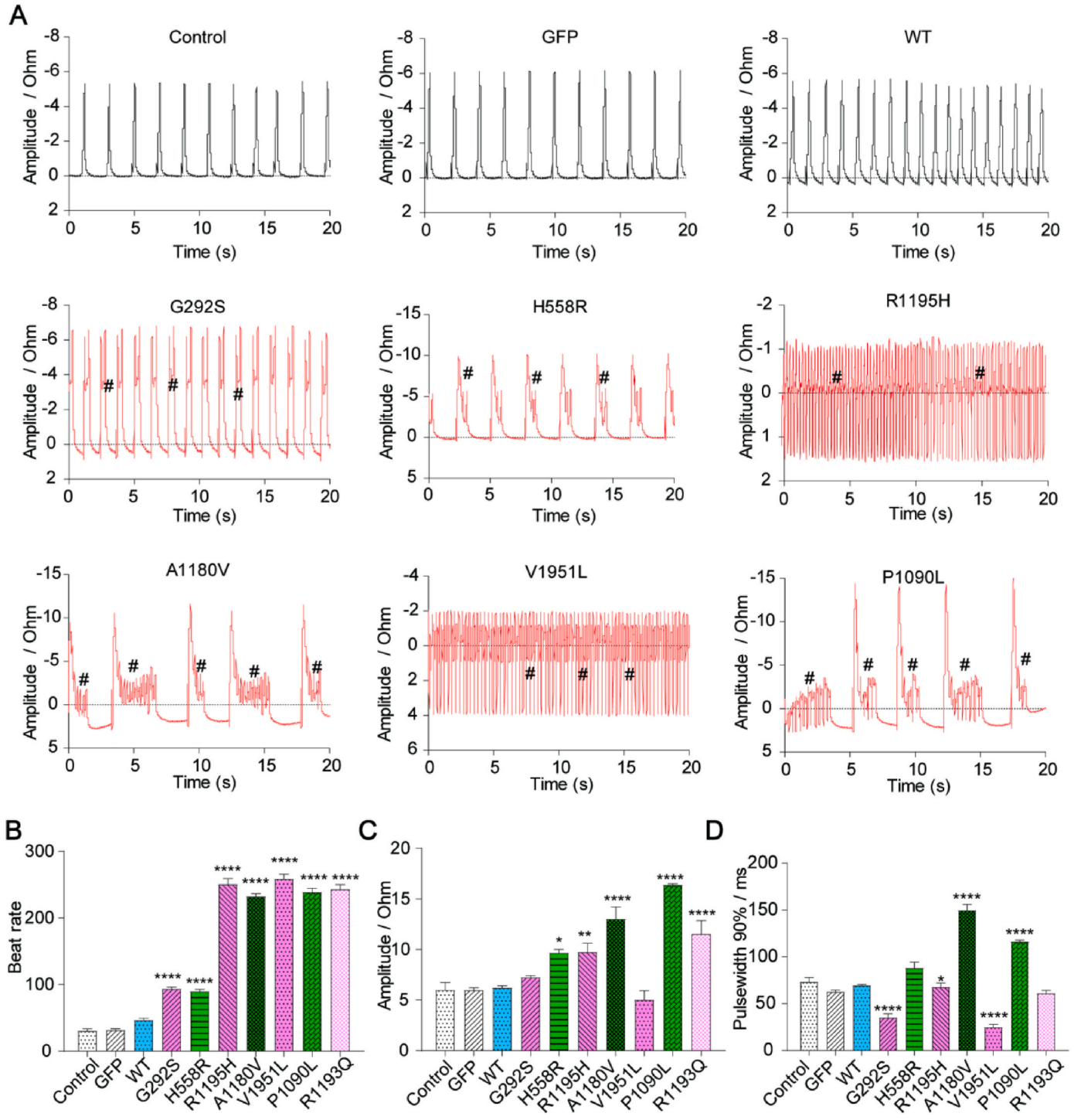

Fig. 4. Effects of NaV1.5 WT and variant NaV1.5 on the contraction of hESC-CMs.
A Representative traces of impedance detected by the CE96 system in the WT, variant and control groups. *SCN5A* variants induce a secondary beat and degenerate into fibrillation. #: secondary beat. **B** Bar graphs showing the beat rate for the WT and variant channel groups. **C** Bar graphs showing the beating amplitude for the WT and variant channel groups. **D** Bar graphs showing the pulse width (90 %) at which the WT and variant channel groups were beating. The data are shown as the mean ± SEM. The details of the beat rate, amplitude and pulse width are provided in Table S3. (***P < 0.001, **P < 0.01, *P < 0.05; one-way ANOVA).

all the *SCN5A* variant cardiomyocytes exhibited arrhythmia-like fibrillation, as indicated by an increase in the secondary beat and the beat rate (Fig. 4A–B). All the amplitudes increased in the variant channel group except for those of the p.V1951L-*SCN5A* variant (Fig. 4C). The pulse widths (90 %) of the p.G292S–*SCN5A* and p.V1951L-*SCN5A* variants were narrower than that of the WT. In contrast, wider pulse widths were observed for the p.H558R–*SCN5A*, p.P1090L-*SCN5A*, and p.A1180V–*SCN5A* variants due to the secondary beat (Fig. 4D), which caused two beats to be counted as one beat. We monitored the extracellular field potential (EFP) after transfection to examine how *SCN5A* mutations affect the length and firing frequency of cardiomyocytes. The duration of EFP in the CM variant group was shorter than that in the control group (Fig. 5A), and the fire frequency of EFP in the variant group increased (Fig. 6A). Detailed information on the beat rate, amplitude, and pulse width is provided in Table S2.

Lidocaine (100 μM) was applied to rescue this arrhythmia phenotype. After 30 min, the percentage of cardiomyocytes with the *SCN5A* variant significantly slow down, and the incidence of the secondary beat also decreased (Fig. 7A–C); this was also the case for G292S (for p.G292S–*SCN5A*: 71.13 ± 2.55 VS 35.08 ± 0.29, ***p < 0.001). These results suggested that Lidocaine could partially correct the fibrillation and secondary beat caused by *SCN5A* variants (Fig. 7A–C). Interestingly, this phenomenon could disappear because of the removal of Lidocaine in all variant groups. This shows that Lidocaine is reversibly bound to channels to play a role in this process. A similar drug effect was observed for most of the *SCN5A* variants, except for the p.H558R–*SCN5A* variant. Lidocaine (100 μM) caused a conduction block in the p.H558R–*SCN5A* variant group (Fig. 7A). The impedance traces of the other p.G292S–*SCN5A*, WT, p.R1193Q-*SCN5A* and control (GFP) groups are provided in Supplementary Fig. S1. The details of the beat rate and amplitude after incubation with Lidocaine are provided in Table S3.

4. Discussion

In our study, among the 27 sporadic LVNC patients, 12 patients had *SCN5A* mutations according to Exome sequencing and analysis. Surprisingly, all 12 LVNC patients with mutations had clinical features consistent with ventricular tachycardia, and some patients presented with abnormal Q waves and prolonged QT intervals. Table 1 shows the detailed clinical features of the patients. The finding that 44.4 % (12/27) of the LVNC patients carried *SCN5A* variants and all presented clinical manifestations of arrhythmia was highly consistent with the findings of a previous publication, which reported that *SCN5A* mutations occurred at a greater rate in LVNC patients with clinical features of arrhythmia or heart failure [18,22]. In fact, seven *SCN5A* mutations have been shown to be associated with arrhythmia diseases by affecting the electrophysiological characteristics of the channel in previous reports. For instance, the variant G292S has been found in Japanese patients with Brugada syndrome [23]. The polymorphism variant H558R was reported to increase the risk of developing atrial fibrillation [24]. V1951L was

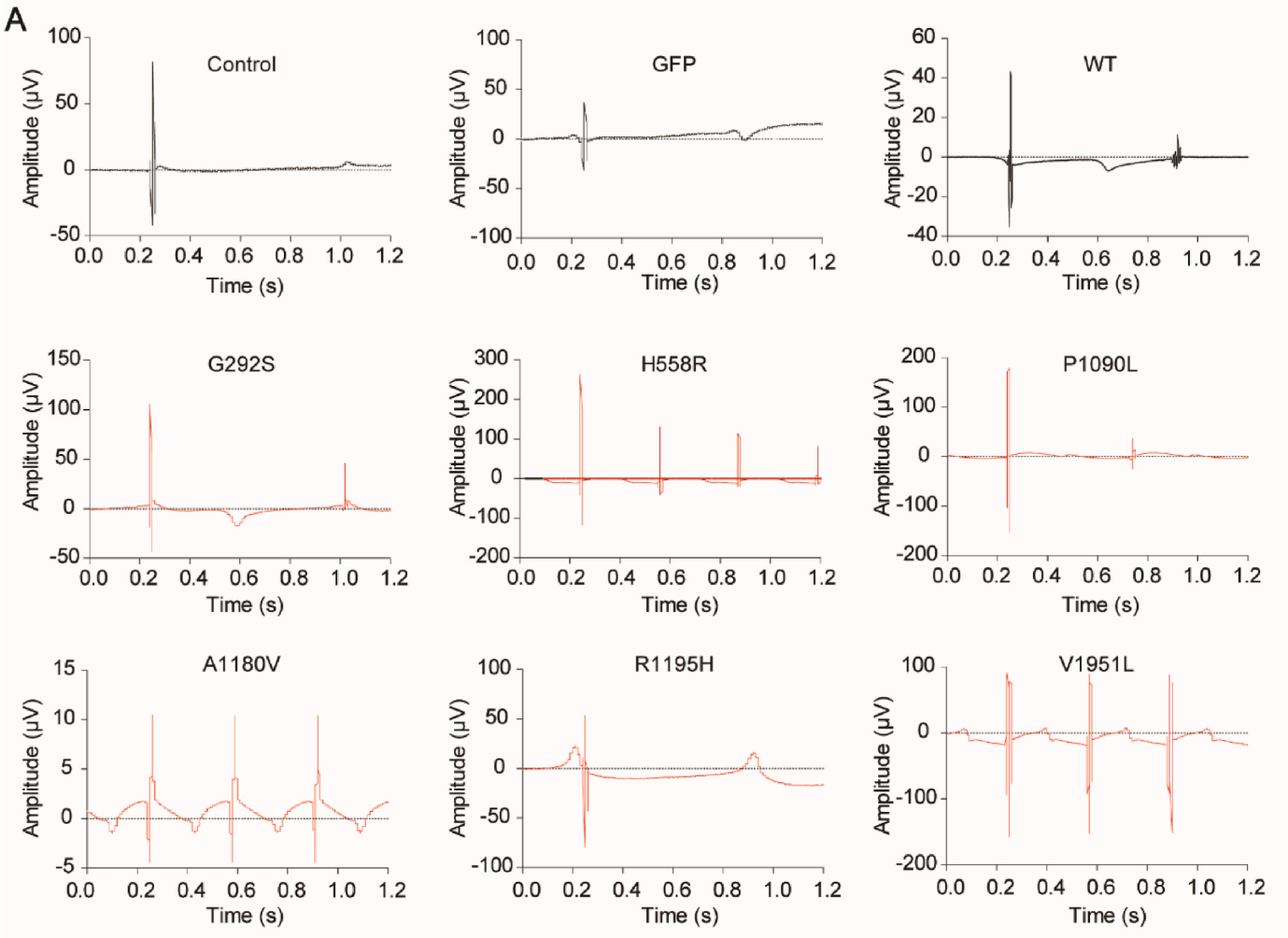

Fig. 5. Effects of NaV1.5 WT and variant NaV1.5 on the extracellular field potential (FP)
A Representative multielectrode array traces of the mean extracellular field potential detected by the CE96 system in the WT, variant and control groups.

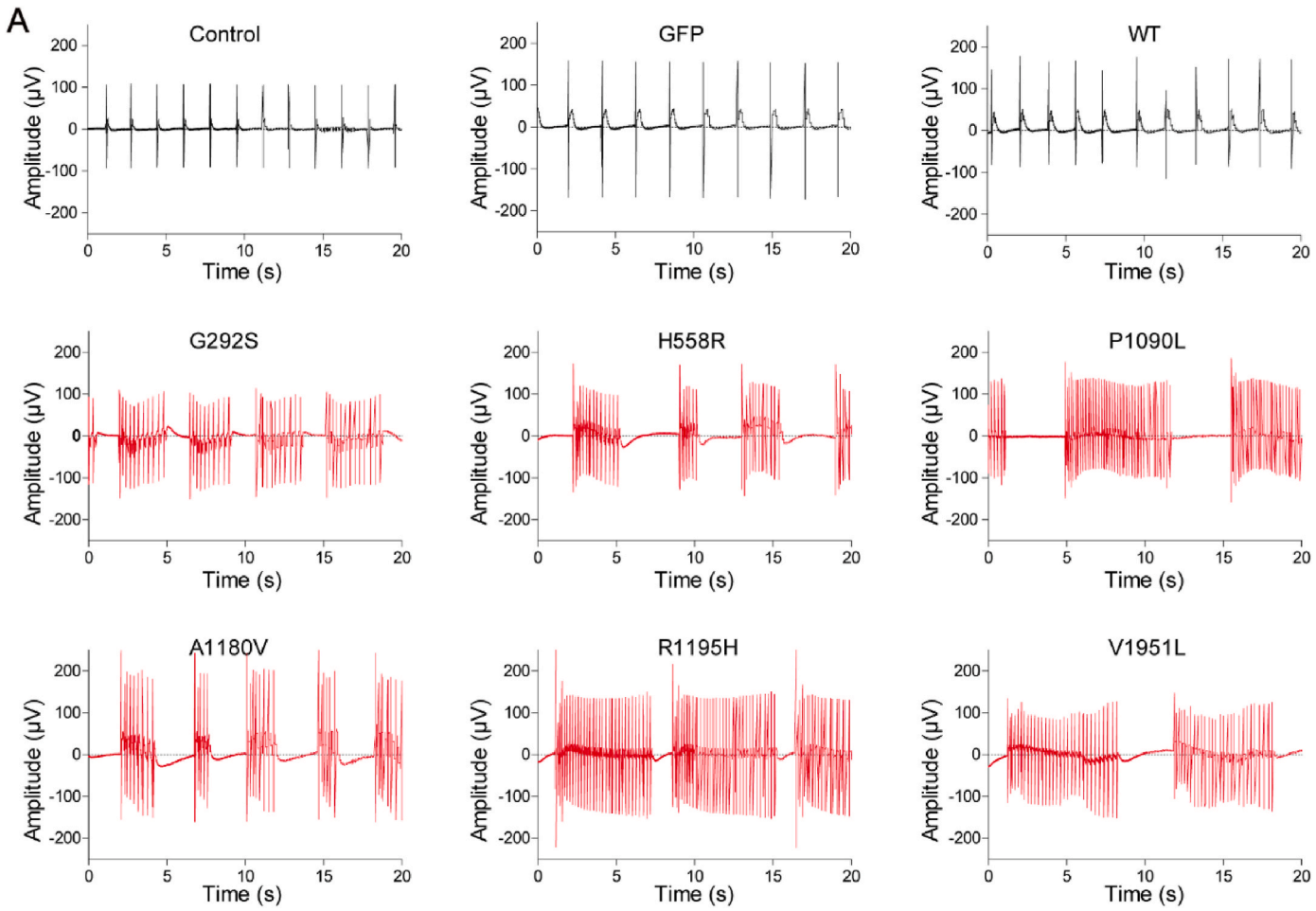

Fig. 6. Effects of NaV1.5 WT and variant NaV1.5 on the frequency of field potentials in hESC-CMs.
A Representative traces of extracellular field potential emission detected by the CE96 system in the WT, variant and control groups.

associated with sudden infant death syndrome [25], and A1180V was a high risk factor for dilated cardiomyopathy with preceding atrioventricular block [26]. P1090L and R1193Q are associated with BrS and LQT3 [27,28]. R1195H is reported in patients with QT prolongation and ventricular arrhythmias [29]. These variants reportedly affect the QT duration or increase the excitability of cardiomyocytes and can lead to arrhythmia in patients with cardiomyopathy. Therefore, we speculate that *SCN5A* mutations may increase the susceptibility of LVNC patients to arrhythmia. We systematically and comprehensively analyzed the electrophysiological characteristics of these patients via the whole-cell patch clamp technique. The physical characteristics of channel activation and fast inactivation control the activity of cardiac sodium channels and contribute to the formation of a cardiac action potential plateau. In contrast, slow inactivation promotes cell excitability through activity-dependent changes that affect the availability of resting channels [20,21]. Our studies revealed that these mutations led to enhanced channel activation and fast activation. All the mutations resulted in a significantly reduced probability of steady-state slow inactivation in both the CHO–K1 (Fig. 3G) and cardiomyocyte models (data not shown). The alterations we observed in slow inactivation suggested an increase in channel availability after an extended period of depolarization. A decreased probability of steady-state slow inactivation of channels increases the fraction of channels available for activation and further increases cell excitability. This is exactly what is happening; we found an increase in EFP firing frequency and beat in hESC-CMs infected with CMs-*SCN5A* variants by the MEA technique. Cardiac myocyte excitability was increased. Some mutations (A1180V, H558R and P1090L) even led to ventricular fibrillation-like arrhythmia and secondary beats in myocardial cells (Fig. 4A). Additionally, we found that Lidocaine (100 μM, except for the p.H558R–*SCN5A* variant, lidocaine (100 μM) could decrease the occurrence rate of secondary beats and alleviate the arrhythmias caused by *SCN5A* variants after incubating for 30 min. Lidocaine caused conduction blockade in the p.H558R–*SCN5A* variant cardiomyocyte group (Fig. 7A). We speculated that the p.H558R–*SCN5A* variant was more sensitive to Lidocaine. In fact, Lidocaine occasionally has side effects of arrhythmias, hypotension, and bradycardia in clinical use [30]. In fact, the p.H558R–*SCN5A* variant is indeed a polymorphism locus and has a high prevalence in the population. Therefore, the necessity of evaluating drug toxicity and effectiveness in cardiomyocytes should be considered, especially for those with polymorphic loci. The locus polymorphic genotype might be ignored and considered harmless in the population. However, severe drug reactions might even occur in the clinic. Understanding the correlation between the inherent mechanism of arrhythmia and these genetic mutations is crucial for advancing the development of innovative pharmaceuticals and facilitating the judicious application of therapeutic interventions.

Our study has several limitations. However, compared with induced iPS cells or gene-edited stem cells, adenovirus-infected CMs could quickly establish mutant cell models. This approach cannot accurately control the exogenous expression level of the variants, so the variant cardiomyocytes only exhibited a stable arrhythmia phenotype within a certain time window (approximately 24 h). The data are not shown. Therefore, real-time monitoring and observation of cardiomyocyte excitability and contractility are rough and convenient methods for

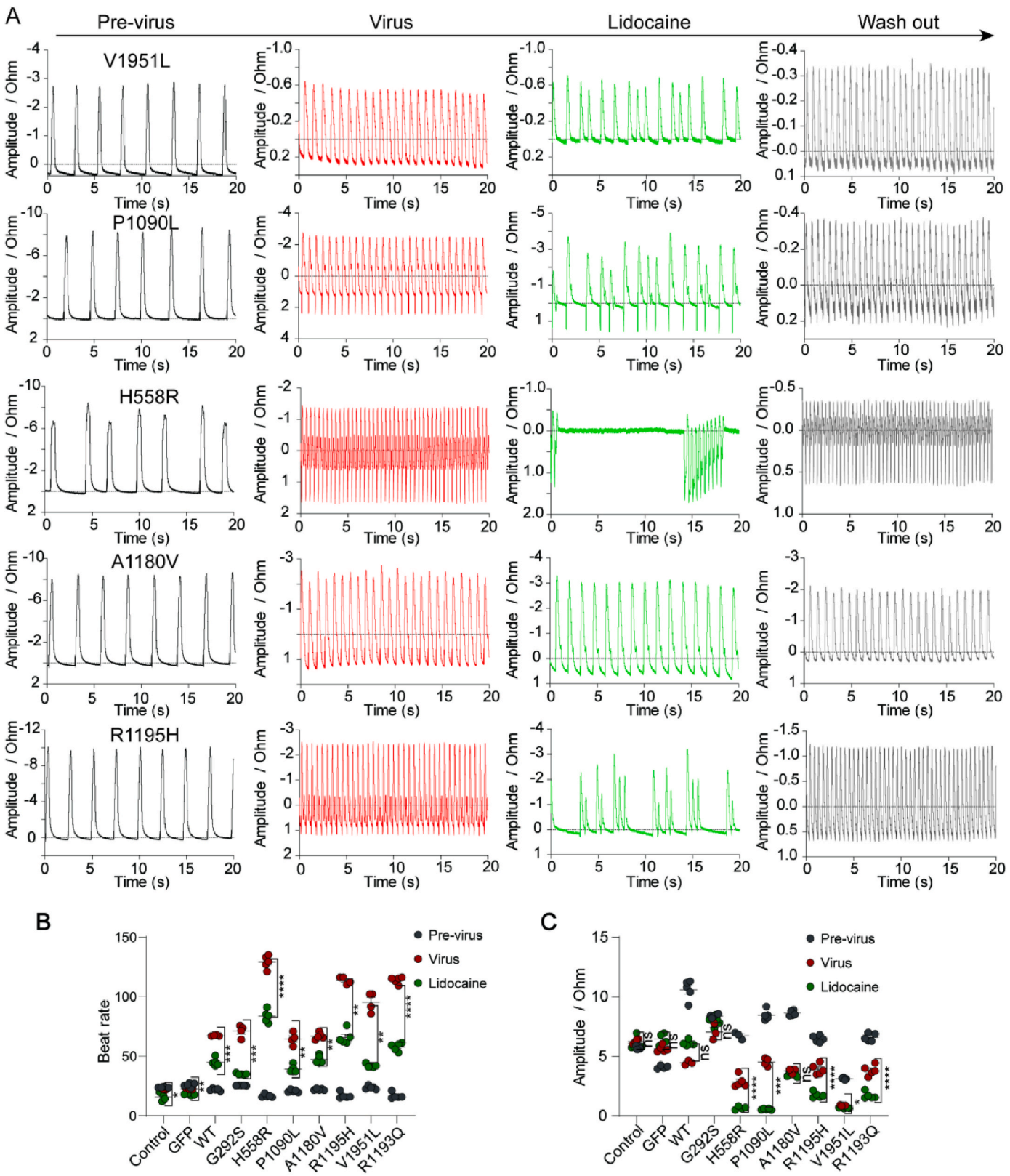

Fig. 7. Acute cardiac effects of Lidocaine, an I_{Na} ion channel modulator and antiarrhythmic drug on cell contraction in the variant-SCN5A group.
A Cardiac contractility was assessed by examining changes in beat rate and amplitude. The expected acute effects of cardiac ion channel modulators of I_{Na} (Lidocaine,100 μM) were confirmed by the traces above showing spontaneous contractile activity under control conditions (pre-drug) and in the presence of the drug after 30 min of incubation. Lidocaine can slow the acceleration and fibrillation of hESC-CMs caused by *SCN5A* variants. **B** The scatter plot shows the effect of 100 μM Lidocaine on the beat rate of hESC-CMs. **C** The scatter plot illustrates the impact of a concentration of 100 μM Lidocaine on the beat amplitude of human embryonic stem cell-derived cardiomyocytes (hESC-CMs). #: secondary beat. The data are shown as the mean ± SEM. The details of the beat rate and amplitude are provided in Table S3.

studying the intrinsic mechanism of arrhythmias and drug screening evaluation platforms.

5. Conclusions

The findings of our study indicate a high prevalence of pathogenic *SCN5A* variants in patients with left ventricular non-compaction (LVNC). Specifically, we confirmed that these variants result in increased activation and inactivation of NaV1.5 in CHO–K1 cells. Additionally, we demonstrated that these variants enhance the excitability and contractility of cardiomyocytes in hESC-CMs models. Moreover, our research highlights the feasibility and convenience of using adenovirus-mediated transfection in hESC-CMs models to investigate the underlying mechanisms of disease, conduct drug screening, and evaluate cellular-level effects. Overall, our data provide a robust and credible explanation for the electrophysiological mechanisms through which *SCN5A* mutations may contribute to the development of a cardiomyopathic phenotype and ventricular tachycardia in LVNC patients.

Funding source

This work was supported by the CAMS Initiative for Innovative Medicine (CAMS-I2M, 2016-I2M-1–015 to Y.J. Wei) and the National Natural Science Foundation of China (grant no. 81470424).

CRediT authorship contribution statement

Yanfen Li: Writing – original draft, Writing – review & editing, Data curation, Investigation. **Shenghua Liu:** Data curation, Formal analysis. **Jian Huang:** Methodology. **Yuanyuan Xie:** Data curation, Investigation. **Aijie Hou:** Writing – review & editing. **Yingjie Wei:** Funding acquisition, Writing – review & editing.

Declaration of competing interest

The authors declare that they have no known competing financial interests or personal relationships that could have appeared to influence the work reported in this paper.

Acknowledgment

We are grateful for the generous donation of human NaV1.5 cDNA from Dr. Zhao-bing GAO (Shanghai Institute of Materia Medica, Chinese Academy of Sciences, Shanghai, China).

Appendix A. Supplementary data

Supplementary data to this article can be found online at https://doi.org/10.1016/j.bbrep.2024.101653.

References

[1] B.J. Maron, J.A. Towbin, G. Thiene, B.J. Maron, J.A. Towbin, G. Thiene, B. J. Maron, J.A. Towbin, G. Thiene, Contemporary Definitions and Classification of the Cardiomyopathies, Circulation 113 (2006) 1807–1816.
[2] T.K. Chin, J.K. Perloff, R.G. Williams, K. Jue, R. Mohrmann, Isolated noncompaction of left ventricular myocardium. A study of eight cases, Circulation 82 (1990) 507–513.
[3] Habib Gilbert, Philippe, Isolated left ventricular non-compaction in adults: clinical and echocardiographic features in 105 patients. The results. Results from a French registry, Gilbert, Habib, Philippe, Gilbert, Habib, Philippe, Eur. J. Heart Fail. 13 (2014) 177–185.
[4] M. Hasegawa, M. Taira, T. Kanaya, K. Araki, Y. Sawa, Clinical Outcomes for Children with left ventricular noncompaction and cardiomyopathy, J. Heart Lung Transplant.: the official publication of the International Society for Heart Transplantation 40 (2021) S285.
[5] B. Cardoso, A. Jeewa, E. Minn, J. Ashkanase, E. Jean-St-Michel, Left ventricular Dilatation impacts heart transplant and death in left ventricular non-compaction cardiomyopathy, J. Heart Lung Transplant. 40 (2021) S272–S273.
[6] A. Bhaskaran, SohaibBennett TimothyVirk, Richard G. Kizana, Saurabh EddyKumar, Electrophysiologic and electroanatomic characterization of ventricular arrhythmias in non-compaction cardiomyopathy: a systematic review, Journal of cardiovascular electrophysiology 32 (2021).
[7] N. Rineiska, S. Komissarova, O. Krasko, I. Haidzel, Left Ventricular Non-compaction Cardiomyopathy: Additional Predictors of Life-Threatening Events for Selecting Patients for Cardioverter-Defibrillator Implantation, EP Europace, 2021.
[8] G. Fazio, G. Corrado, C. Pizzuto, G. Fazio, G. Corrado, C. Pizzuto, G. Fazio, G. Corrado, C. Pizzuto, Supraventricular arrhythmias in noncompaction of left ventricle: is this a frequent complication? Int. J. Cardiol. 127 (2008) 255–256.
[9] J.M. Aronsen, F. Swift, O.M. Sejersted, Cardiac sodium transport and excitation–contraction coupling, Journal of Molecular & Cellular Cardiology 61 (2013) 11–19.
[10] K.J. Kontis, Sodium Channel activation gating is affected by Substitutions of voltage sensor Positive Charges in all four domains, J. Gen. Physiol. 110 (1997) 391–401.
[11] W. Stühmer, F. Conti, H. Suzuki, X. Wang, M. Noda, N. Yahagi, H. Kubo, S. Numa, Structural parts involved in activation and inactivation of the sodium channel, Nature.
[12] H.R. Guy, P. Seetharamulu, Molecular model of the action potential sodium channel, Proc. Natl. Acad. Sci. USA 83 (1986) 508–512.
[13] W. Li, L. Yin, C. Shen, K. Hu, J. Ge, A. Sun, *SCN5A* variants: Association with cardiac disorders, Front. Physiol. 9 (2018) 1372.
[14] Y.Y. Vilin, E. Fujimoto, P.C. Ruben, A novel mechanism associated with idiopathic ventricular fibrillation (IVF) mutations R1232W and T1620M in human cardiac sodium channels, Pflügers Archiv 442 (2001) 204–211.
[15] S. Richards, N. Aziz, S. Bale, D. Bick, S. Das, J. Gastier-Foster, W.W. Grody, M. Hegde, E. Lyon, E. Spector, Standards and guidelines for the interpretation of sequence variants: a joint consensus recommendation of the American College of Medical genetics and Genomics and the association for molecular Pathology, Genetics in Medicine Official Journal of the American College of Medical Genetics 17 (2015) 405–424.
[16] C. Li, F. Liu, S. Liu, H. Pan, H. Du, J. Huang, Y. Xie, Y. Li, R. Zhao, Y. Wei, Elevated myocardial SORBS2 and the underlying implications in left ventricular noncompaction cardiomyopathy, EBioMedicine 53 (2020) 102695.
[17] F. Lan, Andrew S. Lee, P. Liang, V. Sanchez-Freire, Patricia K. Nguyen, L. Wang, L. Han, M. Yen, Y. Wang, N. Sun, Oscar J. Abilez, S. Hu, Antje D. Ebert, Enrique G. Navarrete, Chelsey S. Simmons, M. Wheeler, B. Pruitt, R. Lewis, Y. Yamaguchi, Euan A. Ashley, Donald M. Bers, Robert C. Robbins, Michael T. Longaker, Joseph C. Wu, Abnormal Calcium Handling properties Underlie Familial Hypertrophic cardiomyopathy Pathology in patient-specific induced Pluripotent stem cells, Cell Stem Cell 12 (2013) 101–113.
[18] L.S. Shan, Y.U. Xian-Yi, Y.L. Xing, I. Fukiko, Study of the Relationship between *SCN5A* Variants and Left Ventricular Noncompaction with Heart Failure, Journal of Southeast University(Medical ence Edition), 2012.
[19] J.A.A. B, N.M. D, H.S. E, N.S. D, K.U. B, A.K. D, K.N. F, A.K.A. B, M.H.A. C, A novel *SCN5A* mutation associated with idiopathic ventricular fibrillation without typical ECG findings of Brugada syndrome - ScienceDirect, FEBS (Fed. Eur. Biochem. Soc.) Lett. 479 (2000) 29–34.
[20] Y.Y. Vilin, P.C. Ruben, Slow inactivation in voltage-gated sodium channels: molecular substrates and contributions to channelopathies, Cell Biochem. Biophys. 35 (2001) 171–190.
[21] Y.Y. Vilin, N. Makita, A.L. George, P.C. Ruben, Structural determinants of slow inactivation in human cardiac and skeletal muscle sodium channels, Biophys. J. 77 (1999) 1384–1393.
[22] L. Shan, N. Makita, Y. Xing, L. Shan, N. Makita, Y. Xing, L. Shan, N. Makita, Y. Xing, *SCN5A* variants in Japanese patients with left ventricular noncompaction and arrhythmia, Mol. Genet. Metabol. 93 (2008) 468–474.
[23] H. Niimura, A. Matsunaga, K. Kumagai, et al., Genetic analysis of Brugada syndrome in Western Japan: two novel mutations, Circ. J. 68 (2004) 740–746.
[24] L. Chen, W. Zhang, C. Fang, S. Jiang, H. Li, Polymorphism H558R in the human cardiac sodium channel *SCN5A* gene is associated with atrial fibrillation, J. Int. Med. Res. 39 (2011) 1908–1916.
[25] D.W. Wang, R.R. Desai, L. Crotti, et al., Cardiac sodium channel dysfunction in sudden infant death syndrome, Circulation 115 (2007) 368–376. Jan 23.
[26] J. Ge, A. Sun, V. Paajanen, et al., Molecular and clinical characterization of a novel *SCN5A* mutation associated with atrioventricular block and dilated cardiomyopathy, Circ Arrhythm Electrophysiol 1 (Jun 1 2008) 83–92.
[27] J.M. Juang, T.P. Lu, L.C. Lai, et al., Utilizing multiple in silico analyses to identify putative causal *SCN5A* variants in Brugada syndrome, Sci. Rep. 4 (2014) 3850. Jan 27.
[28] Q. Wang, S. Chen, Q. Chen, et al., The common *SCN5A* mutation R1193Q causes LQTS-type electrophysiological alterations of the cardiac sodium channel, J. Med. Genet. 41 (2004) e66. May.
[29] A. Medeiros-Domingo, B.H. Tan, P. Iturralde-Torres, et al., Unique mixed phenotype and unexpected functional effect revealed by novel compound heterozygosity mutations involving *SCN5A*, Heart Rhythm 6 (2009) 1170–1175. Aug.
[30] K.O. Kim, S. Chung, K. Lee, H. Cho, Profound bradycardia with lidocaine during anesthesia induction in a silent sick sinus syndrome patient, J. Clin. Anesth. 23 (2011) 227–230.